

Fishtail effect and the vortex phase diagram of single crystal $\text{Ba}_{0.6}\text{K}_{0.4}\text{Fe}_2\text{As}_2$

Huan Yang, Huiqian Luo, Zhaosheng Wang and Hai-Hu Wen*

National Laboratory for Superconductivity, Institute of Physics and Beijing National Laboratory for Condensed Matter Physics, Chinese Academy of Sciences, P.O. Box 603, Beijing 100190, P. R. China

By measuring the magnetization hysteresis loops of superconducting $\text{Ba}_{0.6}\text{K}_{0.4}\text{Fe}_2\text{As}_2$ single crystals, we obtained the high upper critical field and large current carrying ability which point to optimistic applications. The fishtail (or second peak) effect is also found in the material, and the position of the vortex pinning force shows a maximum at 1/3 of the reduced field, being consistent with the picture of vortex pinning by small size normal cores in the sample. Together with the resistive measurements, for the first time the vortex phase diagram is obtained for superconductor $\text{Ba}_{0.6}\text{K}_{0.4}\text{Fe}_2\text{As}_2$.

The discovery of high temperature superconductivity in $\text{LaFeAsO}_{1-x}\text{F}_x$ has stimulated enormous interests in the field of superconductivity¹. The family of $\text{REFeAsO}_{1-x}\text{F}_x$ (FeAs-1111 phase) exhibits quite high superconducting transition temperatures with the maximum $T_c = 55$ K for $\text{RE}=\text{Sm}^2$ in electron doped region, as well as 25 K in hole doped $\text{La}_{1-x}\text{Sr}_x\text{FeAsO}^3$. Recently, BaFe_2As_2 compound with new structure (FeAs-122 structure) was reported⁴, and by replacing the alkaline earth elements (Ba, Ca, and Sr) with alkali elements, superconductivity with maximum $T_c = 38$ K was discovered.^{5,6,7} The iron based superconductors have quite high upper critical fields^{8,9} which indicates encouraging applications. Compared with the cuprate system, they have both differences and similarities. Concerning the differences between Fe-based and Cu-based superconductors, they involve mainly the symmetry of the order parameter: the former may have an *s*-wave symmetry, while the latter is *d*-wave like. Another important difference is that the iron based superconductors have smaller anisotropy¹⁰, for example, about 5-6 near T_c in $\text{NdFeAsO}_{0.82}\text{F}_{0.18}$ ¹¹. The anisotropy, as in the case of $\text{YBa}_2\text{Cu}_3\text{O}_{7-\delta}$ (YBCO), is about 7-20 near the optimal doping and strongly dependent on the doping level of the sample¹⁰. The research on the vortex dynamics is a useful tool to make the judgment, and recent works suggest that vortex properties in the two materials seem to be similar to each other.^{11,12,13,14}

For some superconductors, the critical current density obtained from the magnetization hysteresis loops (MHL) increases with the magnetic field after the first peak of penetration field. This is the so-called fishtail effect or second peak effect. This feature has been observed in the clean and high quality single crystals of cuprate superconductors; while in the low T_c superconductors, e.g. Nb_3Sn ¹⁵, MgB_2 ¹⁶, etc, peak effect has been observed near the upper critical field H_{c2} which may be induced by a different mechanism. The anomalous second peak appears at different fields for $\text{REBa}_2\text{Cu}_3\text{O}_{7-\delta}$ (REBCO) bulks (RE=rare earth element) at different temperatures¹⁷, however, the peak position is temperature independent for Bi-based and Tl-based cuprate¹⁸. They may have different origins in REBCO and in Bi- or Tl-based cuprates, and have not got final consensus.

The second peak effect has been observed and reported in polycrystalline samples of the FeAs-1111 phase^{19,20,21,22}. However, it has not been reported in the FeAs-122 phase either in polycrystalline or single crystal samples. The effect thus deserves a detailed investigation on single crystals.

The single crystal $\text{Ba}_{0.6}\text{K}_{0.4}\text{Fe}_2\text{As}_2$ samples were grown by the FeAs self-flux method, and the detailed preparation process was given elsewhere²³. The sample in this work was shaped into a rectangle with the dimensions of 1.054 mm (length) \times 0.548 mm (width) \times 0.038 mm (thickness) for both the magnetic and resistive measurements. The measurements were carried out on a physical property measurement system (PPMS, Quantum Design) with the magnetic field up to 9 T ($H \parallel c$). The temperature stabilization is better than 0.1% at fixed temperatures. The magnetic properties were measured by the sensitive vibrating sample magnetometer (VSM) at the vibrating frequency of 40 Hz with the resolution better than 1×10^{-6} emu. The advantage of this technique is that the data acquisition is very fast with a quite good resolution for magnetization. The magnetic field sweeping rate for the MHL was 100 Oe/s.

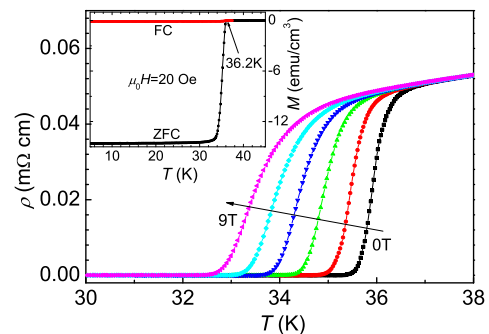


FIG. 1: (Color online) Temperature dependence of resistivity at various fields of 0, 1, 3, 5, 7, 9 T (from right to left) of the $\text{Ba}_{0.6}\text{K}_{0.4}\text{Fe}_2\text{As}_2$ single crystal. The inset shows temperature dependence of the superconducting diamagnetic moment measured in the ZFC and FC processes at a field of 20 Oe.

Fig. 1 shows the temperature dependence of resistivity at various magnetic fields. By taking a criterion of

$95\%\rho_n$, the onset transition temperature at zero temperature is about 36.5 K, while the zero-resistance temperature is about 35.2 K. The diamagnetic transition of the sample is shown in the inset of Fig. 1, which was measured in the field-cooled (FC) and zero-field-cooled (ZFC) processes at a DC magnetic field of 20 Oe. The ZFC curve shows perfect diamagnetism in the low temperature region and the sharp transition with the onset temperature $T_c = 36.2$ K and transition width 1.6 K. Both the magnetic and the resistive measurement indicate good quality of the sample which warrants a further detailed investigation on vortex dynamics. Using the criterion of upper critical field is taken from the resistive transition by $95\%\rho_n$, a huge slope $dH_{c2}/dT = -6.89$ T/K is obtained. The rough estimation of H_{c2} at zero temperature is 174 T by using the Werthamer-Helfand-Hohenberg (WHH) formula²⁴ $H_{c2}(0) = -0.69dH_{c2}(T)/dT|_{T_c T_c}$.

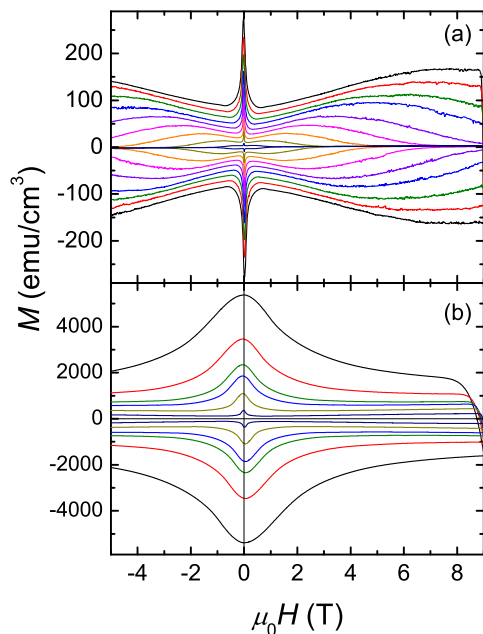


FIG. 2: (Color online) Magnetization hysteresis loops at the temperatures (a) from 27 to 35 K with an interval of 1 K, (b) 2, 5, 10, 15, 20, and 25 K,. Fishtail effect appears in the high field region.

In Fig. 2, the MHL measured at different temperatures from 2 K to 35 K are presented. The symmetric curves suggest that the bulk pinning instead of the surface barrier dominates in the sample. The second peak can be easily observed in Fig. 2 (a) at $T > 27$ K. With the decreasing of T , the peak moves to the high field and finally goes beyond the field region with the maximum value 9 T as shown in Fig. 2 (b). In the region between the valley and the peak, the width of the irreversible magnetization ΔM increases with increasing of the magnetic field, which shows a clear fishtail effect. A

monotonous dropping down of the peak position with increasing temperature can be found in Fig. 2 (b), which suggests that the second peak effect may have the same mechanism as that in REBCO¹⁷. Generally, the field dependence of critical current density J_c can be calculated from the MHL based on the Bean critical state model²⁵ $J_c = 20\Delta M/[w(1 - w/3l)]$, where ΔM was measured in emu/cm^3 , and the length l , the width w of the sample ($w < l$) were measured in cm. Fig. 3 shows the field dependence of J_c . The calculated J_c at 2 K and 0 T reaches 4.7×10^6 A/cm², and J_c at 5 K remains more than 1×10^6 A/cm² at 9 T. So the material shows the good current carrying ability.

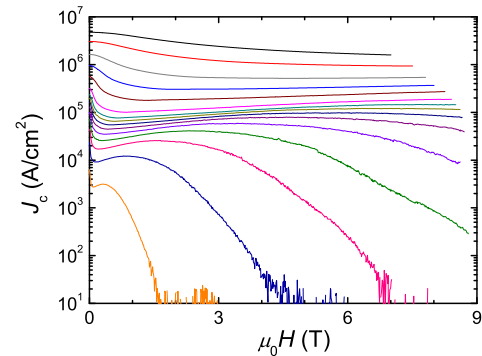


FIG. 3: (Color online) Field dependence of the calculated critical current density from the Bean critical state model at the temperatures corresponding to all the curves in Fig. 2.

In order to find the pinning mechanism of the vortices associating with the fishtail effect, the pinning force density $F_p \propto J_c H$ can provide much information. As proposed by Dew-Hughes²⁶, the pinning force density F_p should be proportional to $h(1 - h)^2$ as the pinning is induced by the small size normal cores. Here h is defined as $h = H/H_{irr}$ where H_{irr} is obtained from the zero value of J_c in $J_c - \mu_0 H$ curves. The expression above yields a maximum value at $h \approx 1/3$. Fig. 4 presents the relationship between normalized pinning force density F_p/F_p^{max} and $h = H/H_{irr}$ of the three curves at high temperatures near T_c . Three curves overlap well with the peak position locating at around $h \sim 0.33$. So the fishtail effect in high temperature region of this sample is from the small size normal cores, which is similar as the results in YBCO.²⁷

In Fig. 5, we present the vortex phase diagram of the material. For the magnetic measurement, three characteristic fields are confirmed as shown by the solid symbols in the inset of Fig. 5. H_{min} and H_{sp} locate at the valley and the peak of the curve, respectively; the irreversibility field H_{irr} is determined by taking a criterion of 10 A/cm². The irreversibility field is also obtained from the zero-resistance temperature in the $\rho - T$ curves shown as open squares in Fig. 5; and the upper critical field H_{c2} with $95\%\rho_n$ are shown as the open circles. The irreversibility lines determined by magnetic and re-

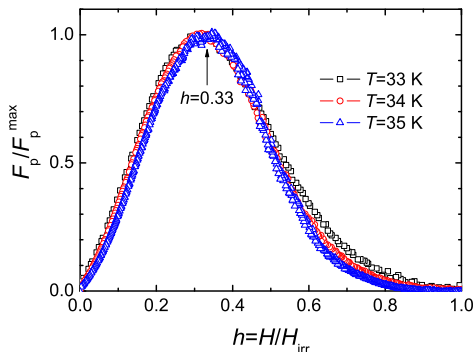


FIG. 4: (Color online) The correlation between the normalized pinning force F_p/F_p^{\max} and the reduced field $h = H/H_{\text{irr}}$. The maximum peak locates at the position $h \sim 0.33$ which is predicted by the theory for the small size normal core pinning.

sistive measurements are slightly different. As $H_{\text{min}}-T$ and $H_{\text{sp}}-T$ curves have more information rather than the linear behavior, we try to find the functional relationship. The two curves are well fitted by the expressions $H_{\text{min}}(T) = H_{\text{min}}(0)(1 - T/T_c)^{1.3}$ with $H_{\text{min}}(0) = 4.0$ T and $H_{\text{sp}}(T) = H_{\text{sp}}(0)(1 - T/T_c)^{1.5}$ with $H_{\text{sp}}(0) = 62.9$ T. The same power-law behavior between H_{sp} and T is found in YBCO²⁸ and the second peak effect is strongly influenced by the oxygen deficiency there. Here in iron based superconductors, the local magnetic moments may form the small size normal cores, and it may be a possible reason of the second peak effect. However, the real pinning mechanism needs further investigation.

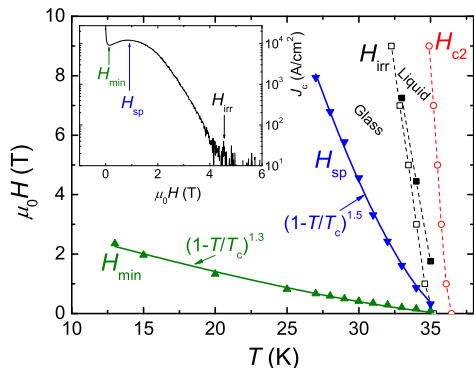


FIG. 5: (Color online) The phase diagram of the $\text{Ba}_{0.6}\text{K}_{0.4}\text{Fe}_2\text{As}_2$ single crystal. The solid symbols are taken from the magnetic measurements (the inset shows the schematic diagram of the definitions of the characteristic parameters), while the open ones are taken from the resistive measurements. The solid lines show the fitting results to the $H_{\text{min}}-T$ and $H_{\text{sp}}-T$ curves.

In conclusion, we find large upper critical field and current carrying ability as well as the fishtail effect in the single crystal $\text{Ba}_{0.6}\text{K}_{0.4}\text{Fe}_2\text{As}_2$. All of them show potential applications of the material. The fishtail effect at high temperatures below T_c is originated from the small size normal core pinning effect as the peak position of pinning force density locates at $0.33H_{\text{irr}}$. The vortex phase diagram of the new material is thus obtained with magnetic field parallel to the c -axis.

This work was financially supported by the Natural Science Foundation of China, the Ministry of Science and Technology of China (973 Projects Nos. 2006CB601000, 2006CB921802 and 2006CB921300), and Chinese Academy of Sciences (Project ITSNEM).

*Electronic mail: hhwen@aphy.iphy.ac.cn.

¹ Y. Kamihara, T. Watanabe, M. Hirano, and H. Hosono, J. Am. Chem. Soc. **130**, 3296 (2008).
² Z. A. Ren, W. Lu, J. Yang, W. Yi, X. L. Shen, C. Z. Li, G. C. Che, X. L. Dong, L. L. Sun, F. Zhou, and Z. X. Zhao, Chin. Phys. Lett. **25**, 2215 (2008).
³ H. H. Wen, G. Mu, L. Fang, H. Yang, and X. Zhu, Europhys. Lett. **82**, 17009 (2008).

⁴ M. Rotter, M. Tegel, D. Johrendt, I. Schellenberg, W. Hermes, and R. Pöttgen, Phys. Rev. B **78**, 020503 (R) (2008).
⁵ M. Rotter, M. Tegel, and D. Johrendt, Phys. Rev. Lett. **101**, 107006 (2008).
⁶ G. F. Chen, Z. Li, G. Li, W. Z. Hu, J. Dong, X. D. Zhang, P. Zheng, N. L. Wang, and J. L. Luo, Chin. Phys. Lett. **25**, 3403 (2008).

- ⁷ K. Sasmal, B. Lv, B. Lorenz, A. Guloy, F. Chen, Y. Xue, and C. W. Chu, *Phys. Rev. Lett.* **101**, 107007 (2008).
- ⁸ F. Hunte, J. Jaroszynski, A. Gurevich, D. C. Larbalestier, R. Jin, A. S. Sefat, M. A. McGuire, B. C. Sales, D. K. Christen, and D. Mandrus, *Nature (London)* **453**, 903 (2008).
- ⁹ Y. Jia, P. Cheng, L. Fang, H. Q. Luo, H. Yang, C. Ren, L. Shan, C. Z. Gu, and H. H. Wen, *Appl. Phys. Lett.* **93**, 032503 (2008).
- ¹⁰ H. H. Wen, *Adv. Mater. (Weinheim, Ger.)* **20**, 3764 (2008).
- ¹¹ Y. Jia, P. Cheng, L. Fang, H. Yang, C. Ren, L. Shan, C. Z. Gu, and H. H. Wen, *Supercond. Sci. Technol.* **21** (2008) 105018.
- ¹² H. Yang, C. Ren, L. Shan, and H. H. Wen, *Phys. Rev. B* **78**, 092504 (2008).
- ¹³ R. Prozorov, M. E. Tillman, E. D. Mun, and P. C. Canfield, *arXiv:0805.2783* (2008).
- ¹⁴ X. L. Wang, S. R. Ghorbani, S. X. Dou, X. L. Shen, W. Yi, Z. C. Li, and Z. A. Ren, *arXiv:0806.1318* (2008).
- ¹⁵ R. Lortz, N. Musolino, Y. Wang, A. Junod, and N. Toyota, *Phys. Rev. B* **75**, 094503 (2007).
- ¹⁶ M. Pissas, S. Lee, A. Yamamoto, and S. Tajima, *Phys. Rev. Lett.* **89**, 097002 (2002).
- ¹⁷ See, for example, U. Welp, W. K. Kwok, G. W. Crabtree, K. G. Vandervoort, and J. Z. Liu, *Appl. Phys. Lett.* **57**, 84 (1990).
- ¹⁸ For Bi-based cuprates, see, for example, Y. Yeshurun, N. Bontemps, L. Burlachkov, and A. Kapitulnik, *Phys. Rev. B* **49**, 1548(R) (1994); see also G. Yang, P. SHang, S. F. Sutton, I. P. Jones, J. A. Abell, and C. E. Gough, *Phys. Rev. B* **48**, 4054 (1993). For Tl-based cuprates, see, for example, V. Hardy, A. Wahl, A. Ruyter, A. Maignan, C. Martin, L. Coudrier, J. Provost, and Ch. Simon, *Physica C* **232**, 347 (1994).
- ¹⁹ C. Ren, Z. S Wang, H. Yang, X. Y. Zhu, L. Fang, G. Mu, L. Shan, and H. H. Wen, *arXiv:0804.1726* (2008).
- ²⁰ J. D. Moore, K. Morrison, K. A. Yates, A. D. Caplin, Y. Yeshurun, L. F. Cohen, J. M. Perkins, C. M. McGilvery, D. W. McComb, Z. A. Ren, J. Yang, W. Lu, X. L. Dong, and Z. X. Zhao, *Supercond. Sci. Technol.* **21**, 092004(R) (2008).
- ²¹ C. Senatore, R. Flükiger, M. Cantoni, G. Wu, R. H. Liu, and X. H. Chen, *Phys. Rev. B* **78**, 054514 (2008).
- ²² A. Yamamoto, A. A. Polyanskii, J. Jiang, F. Kametani, C. Tarantini, F. Hunte, J. Jaroszynski, E. E. Hellstron, P. J. Lee, A. Gurevich, D. C. Larbalestier, Z. A. Ren, J. Yang, X. L. Dong, W. Lu, and Z. X. Zhao, *Supercond. Sci. Technol.* **21**, 095008 (2008).
- ²³ H. Q. Luo, Z. S. Wang, H. Yang, P. Cheng, X. Y. Zhu, and H. H. Wen, *arXiv:0807.0759* (2008).
- ²⁴ N. R. Werthamer, E. Helfand, and P. C. Hohenberg, *Phys. Rev.* **147**, 295 (1966).
- ²⁵ C. P. Bean, *Rev. Mod. Phys.* **36**, 31 (1964).
- ²⁶ D. Dew-Hughes, *Philos. Mag.* **30**, 293 (1974).
- ²⁷ H. H. Wen and Z. X. Zhao, *Appl. Phys. Lett.* **68**, 856 (1996).
- ²⁸ L. Klein, E. R. Yacoby, Y. Yeshurun, A. Erb, G. Müller-Vogt, V. Breit, and H. Wühl, *Phys. Rev. B* **49**, 4403(R) (1994).